

NANO EXPRESS

Open Access



Development of Electrospun Chitosan-Polyethylene Oxide/Fibrinogen Biocomposite for Potential Wound Healing Applications

Tony T. Yuan, Ann Marie DiGeorge Foushee, Monica C. Johnson, Angela R. Jockheck-Clark and Jonathan M. Stahl*

Abstract

Normal wound healing is a highly complex process that requires the interplay of various growth factors and cell types. Despite advancements in biomaterials, only a few bioactive wound dressings reach the clinical setting. The purpose of this research was to explore the feasibility of electrospinning a novel nanofibrous chitosan (CS)-fibrinogen (Fb) scaffold capable of sustained release of platelet-derived growth factor (PDGF) for the promotion of fibroblast migration and wound healing. CS-Fb scaffolds were successfully electrospun using a dual-spinneret electrospinner and directly evaluated for their physical, chemical, and biological characteristics. CS-polyethylene/Fb scaffolds exhibited thinner fiber diameters than nanofibers electrospun from the individual components while demonstrating adequate mechanical properties and homogeneous polymer distribution. In addition, the scaffold demonstrated acceptable water transfer rates for wound healing applications. PDGF was successfully incorporated in the scaffold and maintained functional activity throughout the electrospinning process. Furthermore, released PDGF was effective at promoting fibroblast migration equivalent to a single 50 ng/mL dose of PDGF. The current study demonstrates that PDGF-loaded CS-Fb nanofibrous scaffolds possess characteristics that would be highly beneficial as novel bioactive dressings for enhancement of wound healing.

Keywords: Electrospinning, Biomedical applications, Chitosan, Wound dressing, Fibrinogen, Nanofibers, PDGF, Wound healing

Background

Despite numerous advances made in the field of wound management, few bioactive dressings have been commercialized with the capacity to enhance the healing process. This lack of successful product can be attributed to the complexity of the wound healing process, which involves numerous soluble mediators, blood cells, parenchymal cells, and extracellular matrix (ECM) components. Growth factors play a central role in the wound healing process by promoting cell proliferation, migration, and differentiation. However, rapid elimination and short half-lives in the body [1–3] have limited the clinical adoption of growth factor therapy for promotion of healing and tissue regeneration [4, 5]. Currently,

repetitive in vivo administration of growth factors is required to achieve therapeutic effects (e.g., cellular recruitment and differentiation). The development of a wound dressing that is capable of sustained, localized growth factor delivery would significantly improve treatment outcomes and accelerate clinical adoption.

Platelet-derived growth factor (PDGF) plays a critical role as an initiator and mediator of wound healing; it acts as a chemotactic agent for neutrophils, monocytes, and fibroblasts [6] and helps regulate matrix deposition. In addition, PDGF can inhibit differentiation of fibroblasts into myofibroblasts, which can impact wound contractions and decrease scar formation [6]. PDGF, sold under the brand name Regranex[®], is the only growth factor currently approved by the FDA and is intended for the treatment of lower extremity diabetic ulcers. Once daily topical application of Regranex[®] gel (2.2 μg/cm² of

* Correspondence: jonathan.m.stahl@mail.mil

Naval Medical Research Unit San Antonio, 3650 Chambers Pass, Bldg 3610 BHT-2, JBSA Fort Sam Houston, TX 78234-6315, USA

ulcer) has been shown to result in a 30% faster healing time with minimal adverse effects. However, daily topical application and removal of Regranex® is inconvenient and can adversely impact patient quality of life.

Electrospinning has been established as a notable technique in the fabrication of biomimetic nanofibrous scaffolds using biologically significant polymers. Numerous biodegradable synthetic (e.g., polycaprolactone) and natural polymers (e.g., collagen) have been electrospun into non-woven nanofibrous scaffolds that demonstrate high surface area-to-volume ratios and porosity characteristics, which are important for drug delivery and wound dressing applications. Naturally occurring polymers (e.g., collagen, elastin, and fibrinogen) are particularly attractive wound dressing materials due to their bioactivity, biocompatibility, and unique ability to bind specific growth factors, such as PDGF. Fibrinogen (Fb), a 340-kDa globular plasma protein, plays a major role in clot formation through its activated form, fibrin, which functions as a temporary matrix for tissue repair and regeneration. The absence of Fb and fibrin has been correlated with wound healing defects [7]. Fb-based products demonstrate biodegradability, non-immunogenicity, and cellular migration promotion and have been previously developed as hydrogels [8–10] and wet extrusion cables [11, 12]; however, the physical and structural properties of these materials have limited their clinical adoption. Hydrogels lack structural and mechanical integrity for long-term use, and wet extrusion fibers exhibit exponentially larger diameter sizes (200–250 μm) than the native ECM (200–500 nm). Wnek et al. demonstrated that electrospinning, however, offers the capability to fabricate Fb scaffolds that closely resemble natural ECM structures [13]. Although the resulting nanofibers exhibited improved mechanical properties over hydrogels, the structure still lacked optimum mechanical properties for wound dressing applications [14].

To improve the mechanical properties of electrospun fibrinogen scaffold, additional polymer could be introduced to strengthen the nanofibers [15]. Specifically, chitosan (CS), an *N*-deacetylated derivative of chitin, has been shown to produce desirable antimicrobial properties in wound dressing applications [16, 17]. In addition to being a potent antimicrobial, CS has been electrospun for various biomedical applications including guided bone regeneration [18, 19], transdermal drug delivery [20], directed stem cell differentiation [21], and hemostat [22]. Due to the polycationic nature of chitosan, there are significant difficulties in electrospinning using common solvents. To overcome these difficulties and improve electrospinnability, CS has been mixed with various other polymers such as poly(vinyl pyrrolidone) [23], poly(ethylene oxide) (PEO) [16], and poly(vinyl alcohol) [24]. Similarly, the polycationic

nature of CS has limited successful combination with Fb into a single scaffold due to strong electrostatic interactions. In this work, this limitation was overcome by utilizing a versatile dual-nozzle electrospinning system. The resultant nanofibrous scaffolds were analyzed using various physiochemical characterizations. We hypothesized that the novel combinatory CS-Fb nanofibrous scaffold would present a viable candidate for a bioactive and biomimetic wound dressing that could deliver PDGF and could be effective in influencing fibroblast migration required for wound healing.

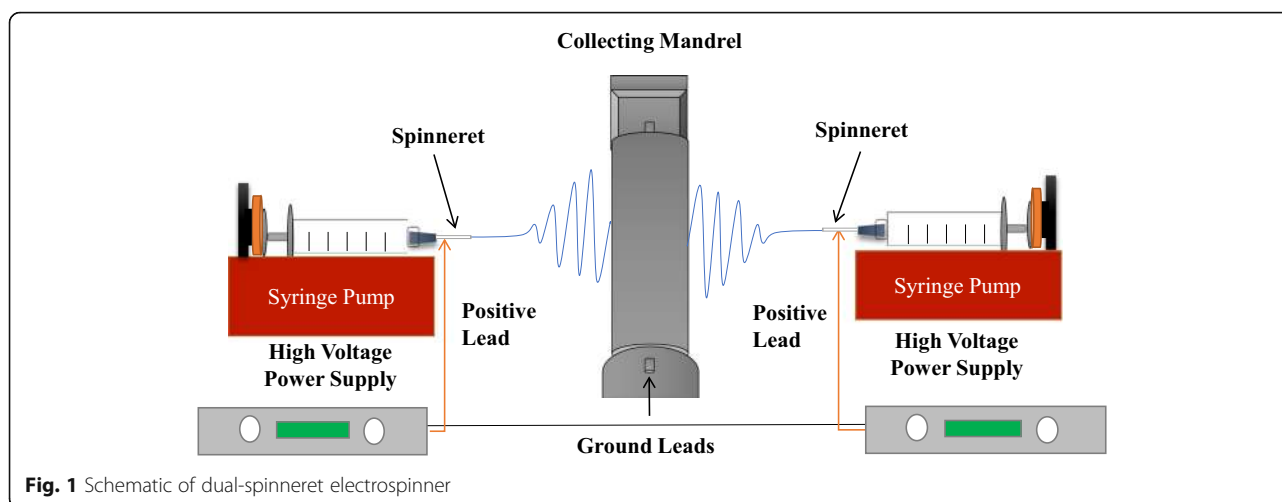
Methods

Materials

Acetic acid (glacial, $\geq 99.85\%$), CS (low molecular weight, 75–85% deacetylation), PEO (MW 300,000 g/mol), Fb (type I-S, 65–85% protein), 1,1,1,3,3,3-hexafluoroisopropanol (HFIP), and bovine serum albumin (BSA, $\geq 96\%$) were purchased from Sigma-Aldrich (St. Louis, MO, USA). Dimethyl sulfoxide (DMSO) was purchased from EMD Millipore (Billerica, MA, USA). Human dermal fibroblasts (PCS-201-012) and cell culture reagents were purchased from American Type Culture Collection (Manassas, VA, USA). Carrier-free recombinant human platelet-derived growth factor-BB (rhPDGF-BB) was purchased from PeproTech (Rocky Hill, NJ, USA). All reagents were of reagent grade and used without further purification or modification.

Preparation of Electrospun Chitosan-Polyethylene Oxide/Fibrinogen Composite Scaffolds

Chitosan-PEO stock solutions were made by dissolving CS and PEO in 1% acetic acid with BSA (0.5% *v/v*) and DMSO (10% *v/v*) to obtain a total polymer content of 5.5 wt.% with a mass ratio of 2:1 CS to PEO. Polyethylene oxide was added to improve the ability to electrospin CS as described previously [16]. Fibrinogen stock solutions (110 mg/mL) were made by dissolving Fb in one-part 10 \times Eagle's minimum essential media (EMEM) and nine parts HFIP. CS-PEO and Fb stock solutions were stirred at room temperature until completely dissolved. For loaded scaffolds, PDGF was mixed into each polymer solution immediately before electrospinning. Electrospun CS-PEO/Fb composite nanofibrous scaffolds were fabricated using a multi-nozzle electrospinning system (Fig. 1). Solutions were individually loaded and mechanically pumped into the system using a disposable syringe, connected to an 18-gauge spinneret and NE-1000 syringe pump (New Era Pump Systems, Farmingdale, NY), at a flow rate of 0.7 and 1.0 mL h⁻¹ for CS-PEO and Fb, respectively. The mandrel collector, rotating at 25 RPM, was located between the spinneret tips at a distance of 22 cm for CS-PEO and 12.5 cm for Fb. During the fabrication process, DC voltages of 28



and 22 kV were applied to the spinneret tips for CS-PEO and Fb polymer solutions, respectively. Fabricated nanofiber scaffolds were either collected on 18-cm glass coverslips for biological assays or directly cut from the mandrel for permeability and tensile strength analysis. All electrospinning experiments were performed at room temperature and a relative humidity of 35–45% for 3 h. Samples containing PDGF were stored at $-20\text{ }^{\circ}\text{C}$ in a desiccator, while unloaded scaffolds were stored in a desiccator at room temperature after fabrication.

Nanofiber Morphology and Diameter

Electrospun nanofibrous scaffolds were sputter-coated with gold and observed using field emission scanning electron microscopy (FESEM) (Zeiss Sigma VP-40, Germany). Twenty micrographs were taken per scaffold, and three individually spun scaffolds were analyzed per formulation. Mean nanofiber diameters were calculated by measuring five random points per micrograph using ImageJ (NIH, Bethesda, MD). A total number of 100 measurements were made per scaffold formulation.

Surface Chemistry Characterization

Time-of-flight ion mass spectrometry (ToF-SIMS) was used to analyze the surface chemistry and the polymer component contributions in the scaffold. ToF-SIMS is a sensitive and in-depth surface analytical methodology which assesses the chemical composition of the top nanometer layer of a material by bombardment with high-energy Bi_3^+ clusters under ultra-high vacuum [25, 26]. Secondary ion fragments ejected from the material surface are then analyzed based on their atomic mass to charge (m/z) ratios and used to infer the overall surface chemical composition.

ToF-SIMS analysis was performed by Evans Analytics Group (EAG, Sunnyvale, CA) using a ToF-SIMS IV (Ion-ToF GmbH, Germany) with a bismuth liquid metal ion gun (30 kV). The instrument was operated in an ion

microprobe mode where three positive and negative ion spectra were acquired from each sample. Selected positive and negative ions were mapped over a $50 \times 50\text{-}\mu\text{m}$ raster area with a 2048×2048 -pixel image resolution to provide polymer component mapping of the scaffolds. A normalized intensity, defined as the count of each secondary ion divided by the total count of ions recorded multiplied by 10,000, was reported for each fragment. The mean of three different locations on the surface of six independently fabricated samples was analyzed ($n = 6$). CS-PEO and Fb polymer distribution analyzed by ToF-SIMS was representative of the whole scaffold.

Water contact angles of CS-PEO, CS-PEO/Fb, and Fb scaffolds were determined in accordance with the American Standards for Testing Methods (ASTM) D7334-08. Nanofibrous scaffolds were electrospun onto glass coverslips. A single droplet of distilled water ($2\text{ }\mu\text{L}$) was applied to the surface of the scaffold and the contact angle measured within 30 s using Krüss DSA10 MK2 Drop Shape Analyzer (Krüss, Hamburg, Germany). The measurements were repeated three times at different locations for each sample, and the mean contact angle was calculated. Six independently electrospun scaffolds were analyzed ($n = 6$).

Mechanical Uniaxial Tensile Strength

The mechanical properties of electrospun scaffolds were measured at room temperature using an Instron® E3000 ElectroPuls (Instron, Canton, MA) equipped with a 250-N load cell at a strain rate of 1 mm min^{-1} . The thickness of the samples was measured at six random positions by Keyence 3D Laser Scanning Microscope VK-200 (Keyence, Itasca, IL). The thickness of the scaffolds used for tensile testing was $93.8 \pm 7.4\text{ }\mu\text{m}$. Before the test, the scaffolds were cut into $40 \times 25\text{-mm}$ rectangular specimens. Data obtained were reported and plotted as stress-strain curves, where tensile stress was defined as

the ratio of force to the cross-sectional area of the specimen and where the strain was defined as the change in length over the original length. Young's moduli, tensile stress, and strain-at-break calculations were obtained from stress-strain curves from an average of ten samples per formulation.

Water Vapor Transfer Rate

Water vapor transfer rate of CS-PEO/Fb scaffolds was measured as per the ASTM E96/E96M desiccant method. A total of six independently electrospun specimens were prepared per formulation and placed on the opening of test vessels containing reusable silica gel desiccant at room temperature and a relative mean humidity of $58.2 \pm 5.2\%$. Water vapor transmission rate (WVTR) was calculated from the weight of the test containers measured at different time points over 48 h:

$$\text{WVTR} = \frac{G}{t \times A} \quad (1)$$

where G represents the change in weight of the test container, t is elapsed time, and A is the cross-sectional area of the scaffold.

In Vitro Cell Viability

Indirect cytotoxicity of the scaffolds was evaluated based on an approach adapted from the ISO10993-5 standard test method [27, 28]. Human dermal fibroblasts were cultured at 37 °C and 5% CO₂ in serum-free fibroblast media and refreshed every 3 days. Once the cells reached confluence, they were trypsinized and seeded into 12-well plates (10,000 cells/mL). The following day, media were replenished and nanofibrous scaffolds were introduced. Cell proliferation was monitored over 120 h using a 2-(4-iodophenyl)-3-(4-nitrophenyl)-5-(2,4-disulfo-phenyl)-2H-tetrazolium sodium (WST-1) cell proliferation assay.

Visualization of Fibroblasts

Human dermal fibroblasts were trypsinized and seeded onto CS-PEO, Fb, and CS-PEO/Fb scaffolds. After 24 h of incubation at 37 °C and 5% CO₂, the cells were washed and stained with LIVE/DEAD™ cell viability kit (ThermoFisher Scientific, Waltham, MA, USA) according to manufacturer's specifications. Additionally, adhesion and attachment of human fibroblasts to the scaffold were evaluated by staining with Phalloidin-Atto 565 (Sigma Aldrich and 4',6-diamidino-2-phenylindole dihydrochloride (DAPI; ThermoFisher Scientific) according to manufacturer's specifications. Images were observed and taken using an inverted confocal microscope (Nikon C1, C1EZ, Melville, NY, USA).

In Vitro Degradation

The degradation of CS-PEO/Fb nanofibrous scaffolds was performed in fibroblast basal medium (FBM, ATCC) at 37 °C and 5% CO₂. Scaffolds were immersed in FBM and incubated for 1, 6, 24, or 48 h. The initial dry weight of each scaffold was noted; at each time point, the scaffolds were washed, freeze-dried, and weighed again. The degradation of the scaffold was calculated from the following formula:

$$\text{Degradation}\% = (W_0 - W_t) / W_0 \times 100 \quad (2)$$

where W_0 is the initial weight of the scaffold, and W_t is the weight of the scaffold at respective time point.

PDGF Release and Detection

Eluates, collected from specific time points during in vitro degradation experiment, were assayed using a rhPDGF-BB-specific ELISA Kit (R&D System, Minneapolis, MN). Detected absorbance values were compared to a standard, as specified by the manufacturer's instructions for determination of PDGF concentration. The amount of PDGF detected was normalized to the weight (mg) of the corresponding scaffold used.

Migratory Property of Released Platelet-Derived Growth Factor

Migration of human dermal fibroblasts was evaluated using ORIS™ cell migration assay kit (Platypus Technologies, Madison, WI) to assess PDGF bioactivity. Briefly, fibroblasts treated with mitomycin C (Sigma-Aldrich, St. Louis, MO) were trypsinized and seeded into 96-well plates containing stoppers provided by the manufacturer and incubated at 37 °C and 5% CO₂ overnight. The following day, stoppers were removed creating migration zones to which 100 μL of eluates collected at various time points was added and incubated for an additional 24 h. Freshly prepared 50 ng mL⁻¹ PDGF and basal fibroblast media were used as positive and negative controls, respectively. Fibroblast migration was expressed as a fold change, compared to the migration elicited by the 50 ng mL⁻¹ PDGF treatment. Studies were performed in triplicate in three independent experiments for three loading concentrations (2, 4, and 8 μg/mL).

Statistical Analysis

Continuous data were expressed as means ± standard deviations. Differences among group means were analyzed using one-way analysis of variance (ANOVA). Tukey's multiple comparison test was used to determine which means among a group of means were statistically different. Statistical significance was set at $\alpha = 0.05$. All

data were analyzed using GraphPad Prism (San Diego, CA, USA).

Results and Discussion

The combination of various polymers has been shown to significantly improve the properties of the resulting composite [29, 30]. Combinatory polymer systems effectively allow for the modulation of scaffold strength, flexibility, biodegradation, and drug release kinetics, which are important parameters for wound dressing applications. However, the creation of unique composites can be limited by intrinsic chemical interactions between the constituent polymers. For example, a polymer precipitate was observed to form when mixing negatively charged Fb and positively charged CS; this observation is well-documented for molecules with strong electrostatic interactions under various solvent conditions [31–33]. Consequently, fabrication of a CS-Fb polymer composite scaffold required the use of a dual extrusion electrospinning technique, as previously described [34].

Morphology of CS-PEO/Fb Nanofibers

Mean fiber diameters for CS-PEO, CS-PEO/Fb, and Fb scaffolds were 269.9 ± 68.4 , 202.3 ± 113.2 , and 351.1 ± 101.7 nm, respectively (Fig. 2). Interestingly, CS-PEO/Fb composite scaffolds exhibited thinner nanofibers than either the CS-PEO or Fb scaffolds. The decrease in fiber diameter size could be due to additional electrostatic forces generated by simultaneously charged polymer jets [35–37]. The repulsion of the polymer jets away from one another caused by these forces could therefore increase both the inter-spinneret distance and time of deposition. The resulting extended deposition time correlates with increased bending instabilities that are known to cause fiber elongation and thinner fiber formation.

Surface Chemistry Characterization via ToF-SIMS and Water Contact Angle

The ToF-SIMS spectra from CS, Fb, and PEO scaffolds are shown in Fig. 3. Normally, unique chemical

fingerprint species can be used to distinguish individual polymer components. Due to the chemical similarities between CS and Fb, however, there was a number of nitrogen containing species ($C_3H_6NO^+$, CH_4N^+ , CN^- , and CNO^-) present in both spectra, making it difficult to distinguish the polymers from one another. However, when Fb was incorporated in the scaffold, the total number of CN^- and CNO^- species increased whereas the other fragments remained unchanged or decreased. Therefore, examining changes in CN^- and CNO^- fragment intensities allowed for the indirect detection of Fb. Similarly, the increase of $C_2H_5O^+$ (45 m/z) ions was used to identify the ethylene oxide fragments of the PEO in the composite scaffolds.

To elucidate the presence and distribution of Fb components within the composite scaffolds, CNO^- and CN^- ions were mapped over a 50×50 - μm raster of the pristine and composite scaffolds to obtain heat maps (Fig. 4a, b). The same mapping technique was performed on $C_2H_5O^+$ to determine PEO distribution (Fig. 4c). Increased heat map intensity was correlated with higher polymer content of Fb or PEO. We observed that the intensities of CNO^- , CN^- , and $C_2H_5O^+$ were uniformly distributed throughout the 50×50 - μm raster area of the composite scaffolds. Due to the thickness of the scaffolds (93.8 ± 7.4 μm) and layer-by-layer fiber deposition, the surface composition is expected to be representative of the whole scaffold. Hence, the ToF-SIMS data suggest that when CS-PEO/Fb nanofibrous scaffolds are fabricated using dual-spinneret electrospinning, individual components are deposited uniformly throughout the composite scaffold.

Water contact angles of electrospun CS-PEO, CS-PEO/Fb, and Fb fibrous scaffolds were determined to be $44.2^\circ \pm 5.1^\circ$, $61.4^\circ \pm 7.6^\circ$, and $115.7^\circ \pm 16.2^\circ$, respectively (Fig. 5). Based on the water contact angles, CS-PEO and CS-PEO/Fb scaffolds were hydrophilic ($> 90^\circ$), while Fb scaffolds were hydrophobic ($< 90^\circ$). Water contact angles of CS-PEO/Fb composite scaffolds demonstrated surface characteristics that were between those of its

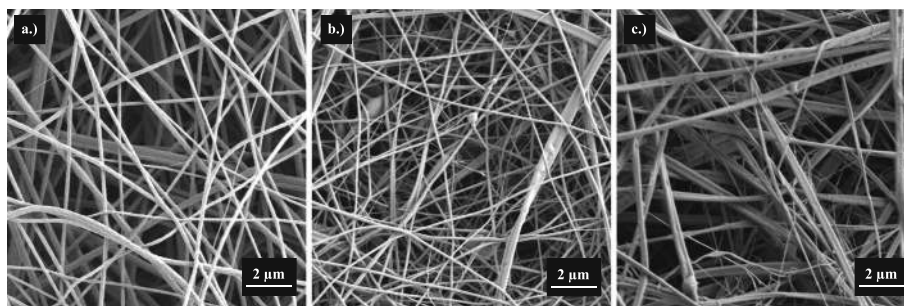


Fig. 2 Representative FESEM micrographs of electrospun scaffolds. **a** CS-PEO, mean diameter 269.9 ± 68.4 nm. **b** CS-PEO/Fb, mean diameter 202.3 ± 113.2 nm. **c** Fb, mean diameter 351.1 ± 101.7 nm ($n = 100$)

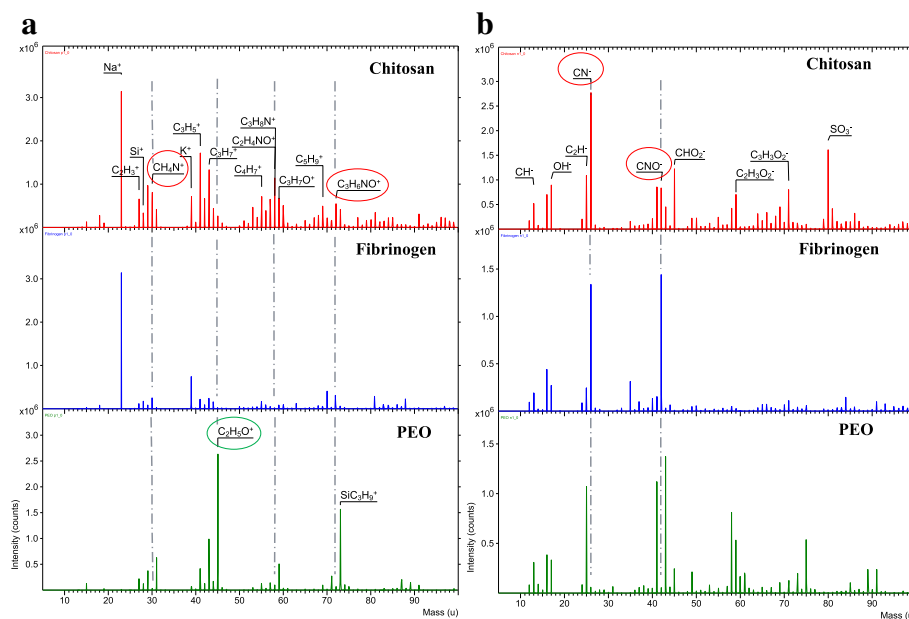


Fig. 3 Representative **a** positive and **b** negative ion ToF-SIMS spectra for pristine CS (top), Fb (middle), and PEO (bottom). Circled ion fragments were utilized as the unique fingerprint to identify the compound

components, which suggest that CS-PEO and Fb were homogeneously deposited during fabrication. Surface characteristics of polymeric surfaces play an important role in the deposition of proteins and adhesion factors. Specifically, important bacterial adhesion factors are known to occur more readily on hydrophobic surfaces, which promote bacterial colonization [38]. As such, the hydrophilic nature of the CS-PEO/Fb might be beneficial in deterring bacterial attachment.

Mechanical Uniaxial Tensile Strength of CS-PEO/Fb Scaffolds

Uniaxial tensile testing was performed on nanofibrous scaffolds with a mean thickness of $93.8 \pm 7.4 \mu\text{m}$. A summary of results is shown in Table 1, and corresponding stress-strain curves are shown in Fig. 6. Generally, mechanical properties of composite materials are correlated with its weakest constituent. Results suggest that Fb-only scaffolds would not have ideal mechanical properties for wound dressing applications. This emphasizes the importance of incorporating CS-PEO to obtain a more mechanically stable product.

Water Vapor Transfer Rate of CS-PEO/Fb Scaffolds

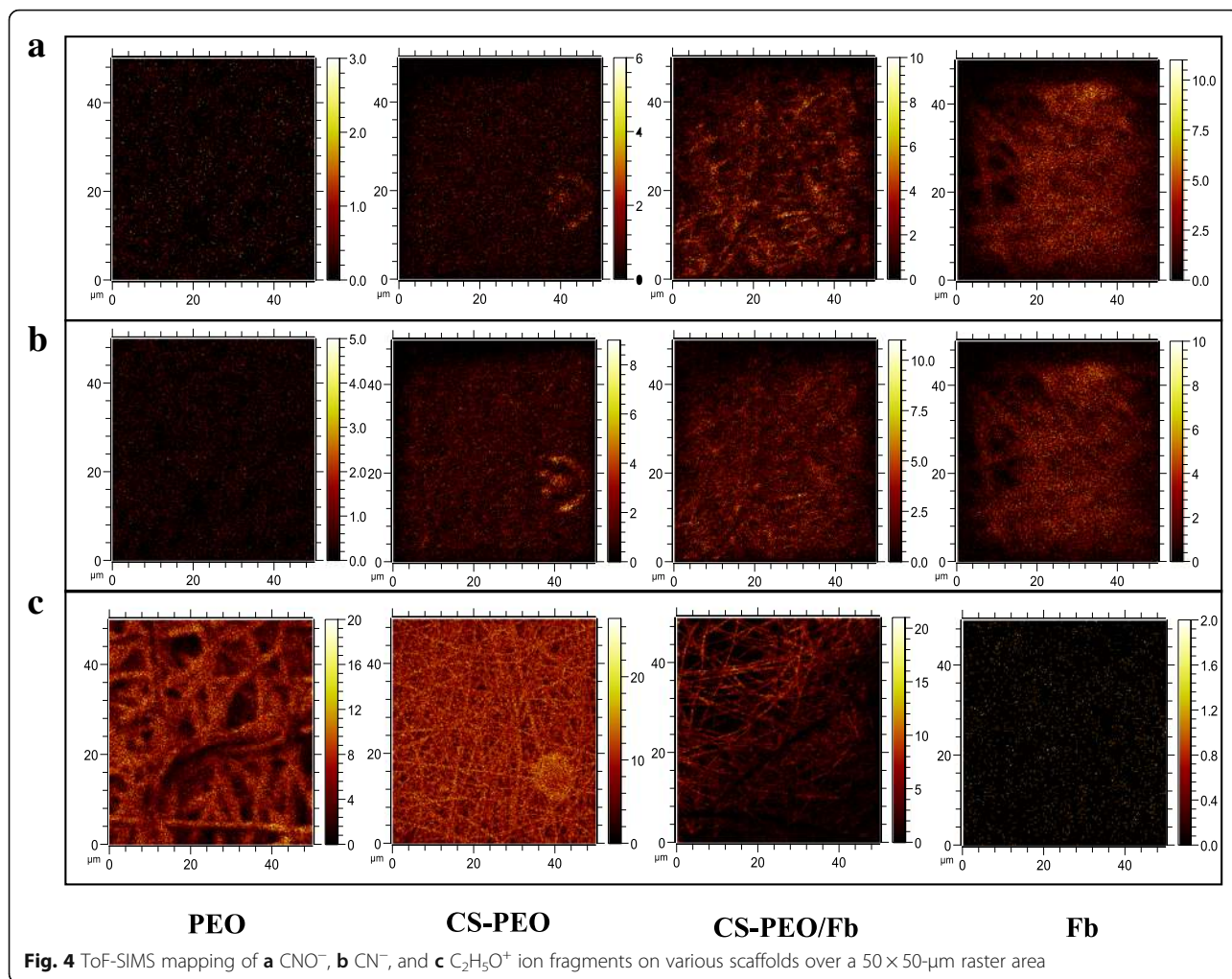
WVTR plays a vital role in maintaining an ideal humidity of the wound environment, which positively impacts cellular granulation and epithelization [39, 40]. Higher WVTR values correlate with rapid wound dehydration due to evaporation and exudation, which can adversely decrease body temperature and increase metabolism.

Conversely, extremely low WVTR values correlate with exudate accumulation, inhibition of healing, and increased risk of infection. Lamke et al. reported the WVTR for normal skin as $204 \pm 12 \text{ g m}^{-2} \text{ day}^{-1}$ and between 279 and $5138 \text{ g m}^{-2} \text{ day}^{-1}$ for injured skin, depending on the condition of the wound [41, 42]. For wound epithelialization and healing enhancement, an ideal WVTR of $2028.3 \pm 237.8 \text{ g m}^{-2} \text{ day}^{-1}$ has been reported [43]. WVTRs of CS-PEO and Fb scaffolds were 693.2 ± 95.7 and $686.1 \pm 44.17 \text{ g m}^{-2} \text{ day}^{-1}$, respectively. Although closer to the ideal WVTR than the pristine scaffolds, CS-PEO/Fb scaffolds ($806.5 \pm 56.1 \text{ g m}^{-2} \text{ day}^{-1}$) still fell below the ideal WVTR (Fig. 7). Manipulations to the physical parameters of the scaffold could improve WVTRs to better mimic reported ideal rates.

In Vitro Cellular Viability of Human Dermal Fibroblasts

Chitosan-PEO/Fb scaffolds did not exhibit a significant proliferative effect on human fibroblasts during the initial 48 h (Fig. 8); yet, prolonged exposure at 72 h produced a statistically significant reduction in proliferation compared to the no scaffold control. The results suggest that there is inhibition of cellular proliferation exhibited by the scaffold, which may be cumulative over time.

The decreased proliferative capacity may be due to the degree of acetylation (DA) associated with CS, which has been shown to have strong cellular interactions through its positive charges [44]. Younes et al. demonstrated bladder carcinoma cells treated with CS (>50% DA) significantly reduced viability after 24 h, suggesting CS



cytotoxicity is directly related to its DA which can impact proliferation [45]. This effect may also be isolated to in vitro experimental conditions; previous studies have shown CS to be non-toxic in vivo, as its biodegradation products could be cleared through metabolic pathways [46]. Residual HFIP from the electrospinning process may also contribute to the observed cytotoxicity. However, the same cytotoxicity was not observed in the electrospun pure Fb scaffold, which was also prepared in HFIP. HFIP was likely eliminated from electrospun

scaffolds during the fabrication process due to its high volatility. An observable decrease in cell viability would be evident if residual HFIP incorporated into the fiber system was being released during timed exposure to human dermal fibroblasts.

LIVE/DEAD Assay and Cellular Attachment

Figure 9a–c shows the distribution and viability of dermal fibroblasts seeded on the surface of fibronectin-coated glass, unloaded CS-PEO/Fb scaffolds, and PDGF-

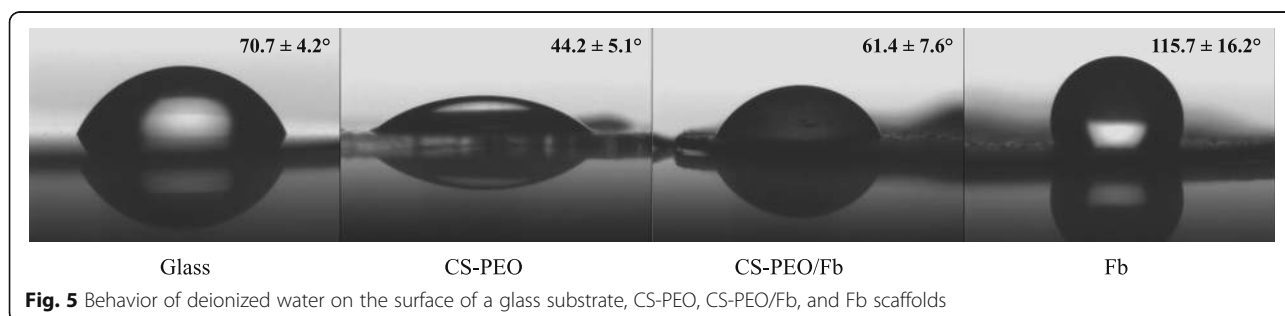


Table 1 Uniaxial tensile properties of electrospun scaffolds ($n = 10$)

Scaffold	Young's modulus (MPa)	Tensile stress (MPa)	Strain at break (%)
CS-PEO	78.12 ± 15.24*	7.27 ± 3.00*	9.88 ± 2.69
CS-PEO/Fb	18.84 ± 5.19	1.28 ± 0.38	8.25 ± 1.70
Fb	6.49 ± 1.89*	0.37 ± 0.10*	26.44 ± 8.58*

Comparisons made to CS-PEO/Fb scaffolds

* $p < 0.05$

loaded (4 $\mu\text{g/mL}$) CS-PEO/Fb scaffolds. After 24 h in culture, minimal dead cells were observed in comparison to the live cells. No discernable differences between PDGF-loaded and unloaded scaffolds were noted.

Fibrinogen serves as an important mediator of cellular attachment and growth during wound healing. Phalloidin stains cellular actin filaments allowing for visualization of fibroblast attachment. Figure 9c, d shows the actin filament morphology of the fibroblasts on the surface of fibronectin-coated glass, unloaded CS-PEO/Fb scaffolds, and PDGF-loaded CS-PEO/Fb scaffolds. Overall, normal fibroblast morphology was observed, with the exception of some rounder cells being present on the scaffold samples. The changes in morphology may be attributed to the presence of CS, as shown in previous studies [47]. Alternatively, the differences could be due to the small porosity of the scaffold and dimensionality of the fiber surface in comparison to the flat surface of the control.

In Vitro Degradation of Electrospun CS-PEO/Fb Scaffolds

Scaffold degradation was evaluated by obtaining the dry weight of the scaffold after incubation in FBM for up to 48 h (Fig. 10). The scaffolds degraded at a linear rate

after an initial burst release of material within the first hour. Weight loss in the initial hour was likely due to the solubility of PEO in aqueous solutions [16], and the subsequent weight loss was likely due to Fb and CS release. This highlights a unique biphasic degradation profile that could be beneficial for the delivery of bioactive molecules. Concurrently, CS-PEO/Fb scaffolds were shown to maintain their substructure for a minimum of 48 h (Fig. 10: insert), and the addition of 8 $\mu\text{g/mL}$ of PDGF did not alter the scaffold degradation properties.

In Vitro Release of PDGF

Cumulative releases of PDGF after 48 h of incubation were 1.8 ± 0.7 , 4.4 ± 1.8 , and 11.4 ± 4.8 ng of PDGF/mg of scaffold for initially incorporated concentrations of 2, 4, and 8 $\mu\text{g/mL}$ of PDGF, respectively. The results demonstrated that PDGF was released from the scaffolds in a dose-dependent manner (Fig. 11).

During the in vitro degradation, CS-PEO/Fb scaffolds exhibited a unique biphasic release profile, with $21.6 \pm 0.1\%$ of the total eluted PDGF being detected in the first hour followed by linear release kinetics. This observation was thought to be a result of the combined polymers and highlighted the functional importance of Fb as a reservoir for the sustained release of biologically critical molecules. Growth factors (e.g., PDGF/VEGF, FGF, and TGF- β families) have been shown to bind the Fb heparin

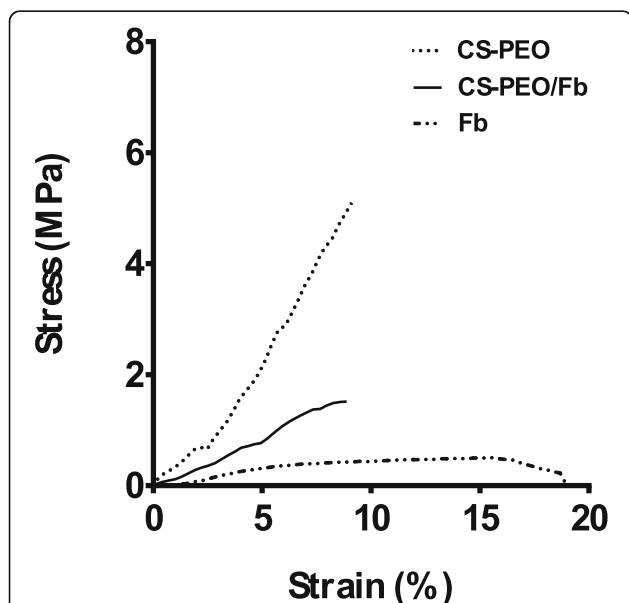


Fig. 6 Stress-strain curves of CS-PEO, CS-PEO/Fb, and Fb scaffolds. Data are representative of ten independently produced scaffolds

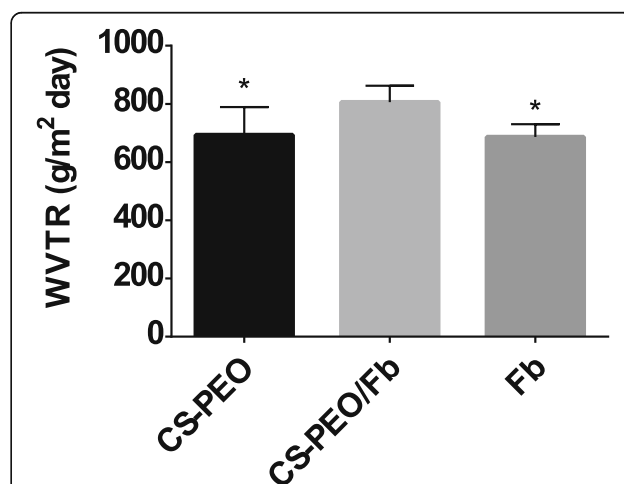


Fig. 7 Water vapor transfer rates of the electrospun CS-PEO, CS-PEO/Fb, and Fb scaffolds. Error bars represent standard deviation ($n = 6$, * $p < 0.05$ when compared to CS-PEO/Fb scaffolds)

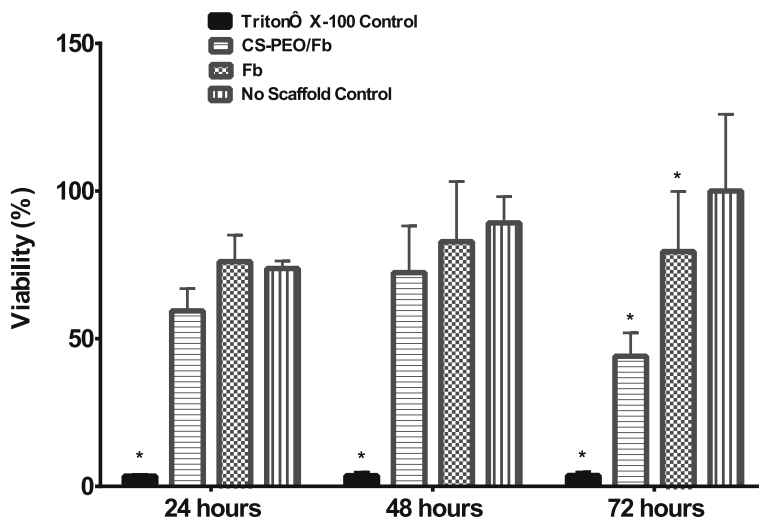


Fig. 8 Comparison of human dermal fibroblast proliferation when exposed to Fb and CS-PEO/Fb electrospun scaffold ($n = 9$, $*p < 0.05$ comparison made to “no scaffold control” at each time point)

domain with high affinity and have been reported to retain their bioactivity for over 7 days [48–50].

Effects of Released PDGF on Fibroblast Migration

Fold differences in fibroblast migration in response to the released PDGF eluates collected from the scaffolds at various time points are shown in Fig. 12. Previously published reports have demonstrated that fibroblast attachment and migration rates are affected by PDGF in a dose-dependent manner [51, 52]. For example, Gamal et al. showed when at least 50 ng/mL PDGF was delivered locally, adherent fibroblast migration was

increased [52]. In addition, Thommen et al. reported that the distance of migration was significantly increased when exposed to PDGF concentrations greater than 10 ng/mL [53]. Therefore, the biological activity of the scaffold-eluted PDGF was measured by its ability to induce migration and was normalized to a single 50 ng/mL PDGF dose.

Eluates collected from electrospun scaffolds, which were loaded with 4 or 8 μg PDGF/mL polymer solutions, demonstrated similar levels of fibroblast migration when compared to a single 50 ng/mL treatment. The data suggest that PDGF delivered by electrospun

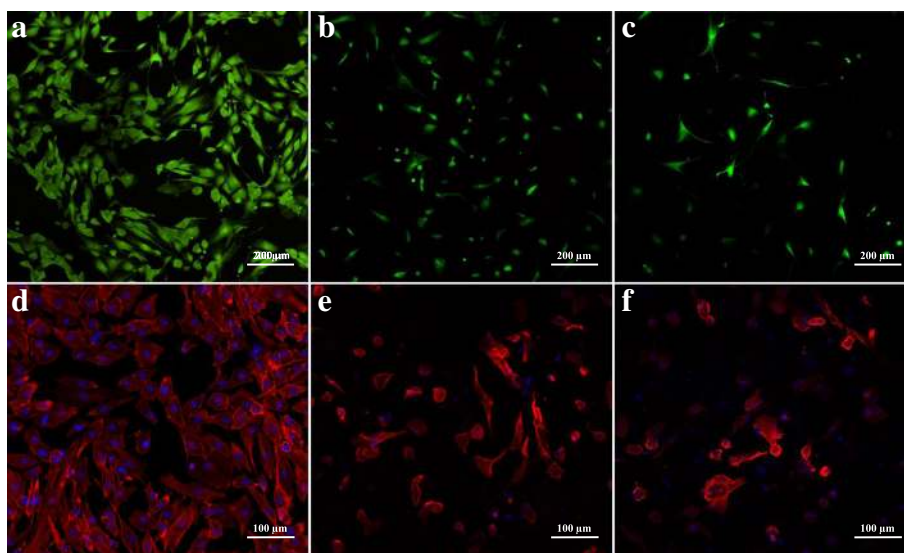
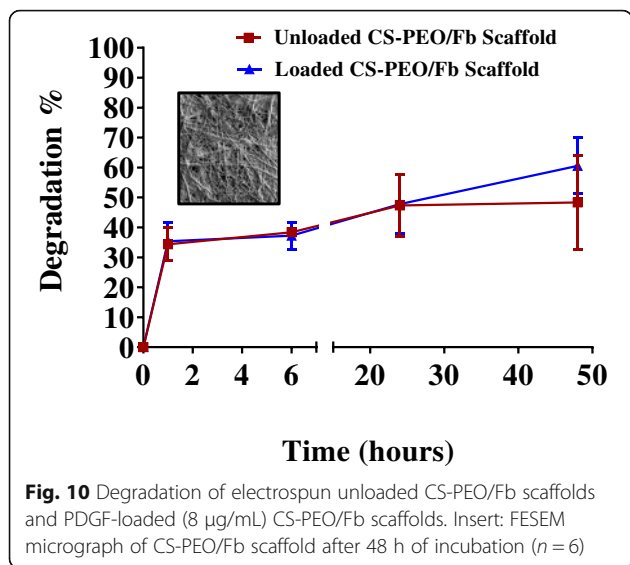
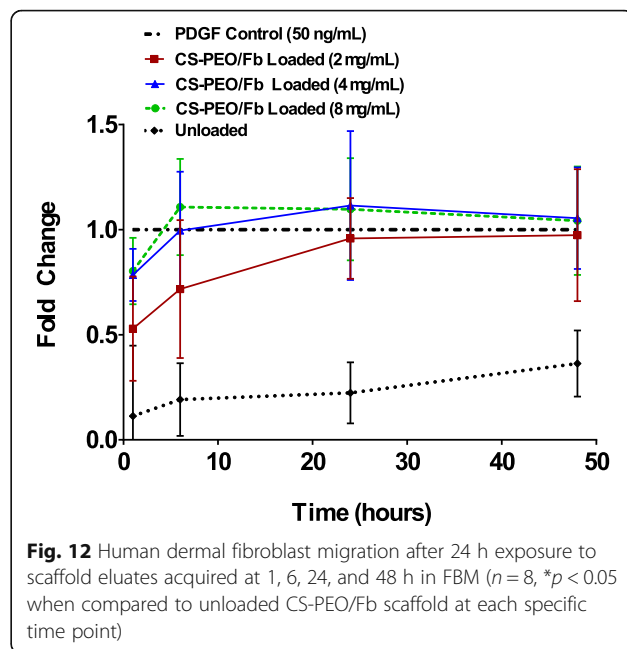
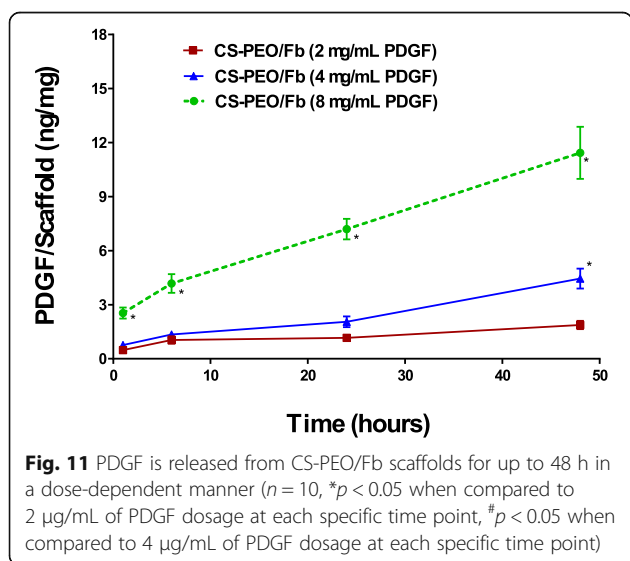


Fig. 9 Confocal micrographs of fibroblasts seeded on **a, d** fibronectin-coated glass; **b, e** unloaded CS-PEO/Fb scaffold; and **c, f** PDGF-loaded (4 μg/mL) CS-PEO/Fb scaffolds. **a–c** Cells were stained with LIVE/DEAD™: live cells (green), dead cells (red). **d–f** Cells were stained with DAPI (blue) and phalloidin (red)



nanofibers can be equally effective in promoting fibroblast migration as a single application of PDGF. Additionally, the migration elicited by the scaffold-released PDGF was sustained for 48 h. Sustained delivery of PDGF eliminates the need for daily applications, which is an advantage over commercially available treatments such as Regranex[®].

Fibroblast migration reached a maximum when cells were treated with the 24-h eluates from each of the PDGF-loaded scaffolds. Notably, when fibroblasts were treated with the 6-h eluates from the 4 and 8 μg PDGF/mL electrospun scaffolds, the same level of maximum migration was achieved. This suggests that the rate of migration increased in response to increased PDGF loading. Additionally, 4 and 8 $\mu\text{g/mL}$ PDGF-loaded scaffolds might be able to elicit fibroblast migration



potentials beyond the detection limits of the current assay, which can only assess the endpoint of migration, but not the migration rate. Finally, results demonstrated that eluates from unloaded CS-PEO/Fb scaffolds were also capable of eliciting a linear increase in migration over the same elution time points, albeit less effectively than the PDGF-loaded scaffolds. This result is most likely mediated by the ability of fibrinogen to enhance fibroblast migration [54, 55]. In general, PDGF-loaded composite scaffolds significantly improved in vitro migration, compared to the individual components of the scaffold.

Conclusion

The versatility of electrospinning allows for the combination of advantageous properties of various polymers and proven bioactive molecules. We utilized this technique to fabricate unique CS-PEO/Fb scaffolds with the ability to release biologically active PDGF over 48 h. This study evaluated the chemical and physical properties of the nanofibrous scaffolds including (1) morphology, (2) physical and mechanical properties, (3) in vitro scaffold degradation, and (4) the ability to release functional PDGF in a dose- and time-dependent manner. Electrospun CS-PEO/Fb scaffolds demonstrated nanoscale morphological properties that are conducive to wound dressing applications, as well as an adequate WVTR, mechanical stability, and a unique biphasic PDGF delivery profile. Furthermore, PDGF maintained its biological function throughout the electrospinning process, and when combined with the natural, chemotactic properties of Fb elicited dermal fibroblast

migration that is functionally equivalent to a single 50 ng/mL dose of PDGF. Overall, these results highlight the potential of CS-PEO/Fb scaffolds as a viable wound dressing capable of delivering bioactive PDGF to enhance fibroblast recruitment and wound healing.

Abbreviations

CS: Chitosan; DA: Degree of acetylation; DMSO: Dimethyl sulfoxide; ECM: Extracellular matrix; EMEM: Eagle's minimum essential media; Fb: Fibrinogen; FBM: Fibroblast blast media; FESEM: Field emission scanning electron microscope; FGF: Fibroblast growth factor; HFIP: 1,1,1,3,3,3-Hexafluoroisopropanol; PDGF: Platelet-derived growth factor; PEO: Polyethylene oxide; PLGA: Poly(lactide-co-glycolide); TGF- β : Transforming growth factor beta; ToF-SIMS: Time-of-flight secondary ion mass spectrometry; VEGF: Vascular endothelial growth factor; WWTR: Water vapor transfer rate

Acknowledgements

The authors would like to thank Dr. Tao You of the US Army Institute of Surgical Research for his valuable contributions on the FESEM images.

Funding

The views expressed in this manuscript are those of the author and do not necessarily reflect the official policy or position of the Department of the Navy, Department of Defense, nor the US Government. This work was funded by Naval Medical Research Center's Advanced Medical Development Program using WUN G1406. The study was approved by the Naval Medical Research Unit San Antonio. The authors are employees of the US Government or military service members. This work was prepared as part of their official duties. Title 17 USC §105 provides that "copyright protection under this title is not available for any work of the US Government." Title 17 USC §101 defines a US Government work as a work prepared by a military service member or employee of the US Government as part of that person's official duties. Approved for public release; distribution is unlimited.

Availability of Data and Materials

All datasets are presented in the main paper or in additional supporting files.

Authors' Contributions

TTY, MCJ, and AMDF designed the experiments. TTY and MCJ prepared the electrospun scaffolds and performed the scaffold degradation experiments. TTY and JMS provided critical insight and analysis of the data. AMDF performed and analyzed the cell experiments related to biocompatibility and migration. ARJC provided critical discussion of the contents and drafting of the manuscript. All authors read and approved the final manuscript.

Authors' Information

TTY, ARJC, and JMS are research scientists at the Naval Medical Research Unit San Antonio. AMDF and MCJ are research associates at the Naval Medical Research Unit San Antonio.

Competing Interests

The authors declare that they have no competing interests.

Publisher's Note

Springer Nature remains neutral with regard to jurisdictional claims in published maps and institutional affiliations.

Received: 11 November 2017 Accepted: 27 February 2018

Published online: 02 April 2018

References

1. Simons M, Annex BH, Laham RJ, Kleiman N, Henry T, Dauerman H et al (2002) Pharmacological treatment of coronary artery disease with recombinant fibroblast growth factor-2 double-blind, randomized, controlled clinical trial. *Circulation* 105(7):788–793
2. Lee KY, Peters MC, Mooney DJ (2003) Comparison of vascular endothelial growth factor and basic fibroblast growth factor on angiogenesis in SCID mice. *J Control Release* 87(1):49–56
3. Post MJ, Laham R, Sellke FW, Simons M (2001) Therapeutic angiogenesis in cardiology using protein formulations. *Cardiovasc Res* 49(3):522–531
4. Sukarto A, Yu C, Flynn LE, Amsden BG (2012) Co-delivery of adipose-derived stem cells and growth factor-loaded microspheres in RGD-grafted N-methacrylate glycol chitosan gels for focal chondral repair. *Biomacromolecules* 13(8):2490–2502
5. Secco M, Bueno C Jr, Vieira NM, Almeida C, Pelatti M, Zucconi E et al (2013) Systemic delivery of human mesenchymal stromal cells combined with IGF-1 enhances muscle functional recovery in LAMA2 dy(2j) dystrophic mice. *Stem Cell Rev Rep* 9(1):93–109
6. Pierce GF, Mustoe TA, Altrock BW, Deuel TF, Thomason A (1991) Role of platelet-derived growth factor in wound healing. *J Cell Biochem* 45:319–326
7. Drew AF, Liu H, Davidson JM, Daugherty CC, Degen JL (2001) Wound-healing defects in mice lacking fibrinogen. *Blood* 97(12):3691–3698
8. Passaretti D, Silverman RP, Huang W, Kirchoff CH, Ashiku S, Randolph MA et al (2001) Cultured chondrocytes produce injectable tissue-engineered cartilage in hydrogel polymer. *Tissue Eng* 7(6):805–815
9. Cummings CL, Gawlitta D, Nerem RM, Stegemann JP (2004) Properties of engineered vascular constructs made from collagen, fibrin, and collagen–fibrin mixtures. *Biomaterials* 25:3699–3706
10. Shreiber DI, Enever PAJ, Tranquillo RT (2001) Effects of PDGF-BB on rat dermal fibroblast behavior in mechanically stressed and unstressed collagen and fibrin gels. *Exp Cell Res* 266:155–166
11. Ahmed Z, Underwood S, Brown RA (2000) Low concentrations of fibrinogen increase cell migration speed on fibronectin/fibrinogen composite cables. *Cell Motil Cytoskeleton* 46:6–16
12. Underwood S, Afoke A, Brown RA, Macleod AJ, Shamlou PA, Dunnill P (2000) Wet extrusion of fibronectin–fibrinogen cables for application in tissue engineering. *Biotechnol Bioeng* 73(4):295–305
13. Wnek GE, Carr ME, Simpson DG, Bowlin GL (2003) Electrospinning of nanofiber fibrinogen structures. *Nano Lett* 3(2):213–216
14. McManus MC, Boland ED, Koo HP, Barnes CP, Pawlowski KJ, Wnek GE et al (2006) Mechanical properties of electrospun fibrinogen structures. *Acta Biomater* 2(1):19–28
15. Cai N, Hou D, Luo X, Han C, Fu J, Zeng H et al (2016) Enhancing mechanical properties of polyelectrolyte complex nanofibers with graphene oxide nanofillers pretreated by polycation. *Compos Sci Technol* 135:128–136
16. Yuan TT, Jenkins PM, DiGeorge Foushee AM, Jockheck-Clark AR, Stahl JM (2016) Electrospun chitosan/polyethylene oxide nanofibrous scaffolds with potential antibacterial wound dressing applications. *J Nanomater* 2016:25
17. Cai N, Li C, Han C, Luo X, Shen L, Xue Y et al (2016) Tailoring mechanical and antibacterial properties of chitosan/gelatin nanofiber membranes with Fe₃O₄ nanoparticles for potential wound dressing application. *Appl Surf Sci* 369:492–500
18. He Y, Liu X, Tang X (2015) In vitro study of electrospun polycaprolactone/chitosan nano fiber membrane guided bone regeneration. *Shanghai J Stomatol* 24(2):129–134
19. Balagangadharan K, Dhivya S, Selvamurugan N (2017) Chitosan based nanofibers in bone tissue engineering. *Int J Biol Macromol* 104:1372–1382
20. Mendes AC, Gorzelanny C, Halter N, Schneider SW, Chronakis IS (2016) Hybrid electrospun chitosan-phospholipids nanofibers for transdermal drug delivery. *Int J Pharm* 510(1):48–56
21. Zhang C, Yuan H, Liu H, Chen X, Lu P, Zhu T et al (2015) Well-aligned chitosan-based ultrafine fibers committed teno-lineage differentiation of human induced pluripotent stem cells for Achilles tendon regeneration. *Biomaterials* 53:716–730
22. Gu BK, Park SJ, Kim MS, Lee YJ, Kim J-I, Kim C-H (2016) Gelatin blending and sonication of chitosan nanofiber mats produce synergistic effects on hemostatic functions. *Int J Biol Macromol* 82:89–96
23. Ignatova M, Manolova N, Rashkov I (2007) Novel antibacterial fibers of quaternized chitosan and poly(vinyl pyrrolidone) prepared by electrospinning. *Eur Polym J* 43(4):1112–1122
24. Zhang Y, Huang X, Duan B, Wu L, Li S, Yuan X (2007) Preparation of electrospun chitosan/poly(vinyl alcohol) membranes. *Colloid Polym Sci* 285(8):855–863
25. Wagner MS, Castner DG (2004) Analysis of adsorbed proteins by static time-of-flight secondary ion mass spectrometry. *Appl Surf Sci* 231:366–376
26. Schilke KF, McGuire J (2011) Detection of nisin and fibrinogen adsorption on poly(ethylene oxide) coated polyurethane surfaces by time-of-flight secondary ion mass spectrometry (ToF-SIMS). *J Colloid Interface Sci* 358(1):14–24

27. Chen J-P, Chang G-Y, Chen J-K (2008) Electrospun collagen/chitosan nanofibrous membrane as wound dressing. *Colloids Surf. A* 313:183–188
28. Charensriwilaiwat N, Opanasopit P, Rojanarata T, Ngawhirunpat T (2012) Lysozyme-loaded, electrospun chitosan-based nanofiber mats for wound healing. *Int J Pharm* 427(2):379–384
29. He Y, Han D, Chen J, Ding Y, Jiang S, Hu C et al (2014) Highly strong and highly tough electrospun polyimide/polyimide composite nanofibers from binary blend of polyamic acids. *RSC Adv* 4(104):59936–59942
30. Zhao R, Li X, Sun B, Zhang Y, Zhang D, Tang Z et al (2014) Electrospun chitosan/sericin composite nanofibers with antibacterial property as potential wound dressings. *Int J Biol Macromol* 68:92–97
31. Zhang W, Zhong D, Liu Q, Zhang Y, Li N, Wang Q et al (2013) Effect of chitosan and carboxymethyl chitosan on fibrinogen structure and blood coagulation. *J Biomed Sci* 24(13):1549–1563
32. Yang J, Tian F, Wang Z, Wang Q, Zeng YJ, Chen SQ (2008) Effect of chitosan molecular weight and deacetylation degree on hemostasis. *J Biomed Mater Res Part B* 84(1):131–137
33. Whang HS, Kirsch W, Zhu YH, Yang CZ, Hudson SM (2005) Hemostatic agents derived from chitin and chitosan. *J Macromol Sci* 45(4):309–323
34. Toncheva A, Paneva D, Manolova N, Rashkov I, Mita L, Crispi S et al (2013) Dual vs. single spinneret electrospinning for the preparation of dual drug containing non-woven fibrous materials. *Colloids Surf A*. 439:176–183
35. Ding B, Kimura E, Sato T, Fujita S, Shiratori S (2004) Fabrication of blend biodegradable nanofibrous nonwoven mats via multi-jet electrospinning. *Polymer* 45(6):1895–1902
36. Thakur R, Florek C, Kohn J, Michniak B (2008) Electrospun nanofibrous polymeric scaffold with targeted drug release profiles for potential application as wound dressing. *Int J Pharm* 364(1):87–93
37. Gupta P, Wilkes GL (2003) Some investigations on the fiber formation by utilizing a side-by-side bicomponent electrospinning approach. *Polymer* 44(20):6353–6359
38. Nagaoka S, Kawakami H (1994) Inhibition of bacterial adhesion and biofilm formation by a heparinized hydrophilic polymer. *ASAIJ* 41(3):M365–M368
39. Korting H, Schöllmann C, White R (2011) Management of minor acute cutaneous wounds: importance of wound healing in a moist environment. *J Eur Acad Dermatol Venereol* 25(2):130–137
40. Field CK, Kerstein MD (1994) Overview of wound healing in a moist environment. *Am J Surg* 167(1):S2–S6
41. Lamke L-O, Liljedahl S-O (1971) Evaporative water loss from burns, grafts and donor sites. *Scand J Plast Reconstr Surg* 5(1):17–22
42. Wu P, Nelson E, Reid W, Ruckley C, Gaylor J (1996) Water vapour transmission rates in burns and chronic leg ulcers: influence of wound dressings and comparison with in vitro evaluation. *Biomaterials* 17(14):1373–1377
43. Xu R, Xia H, He W, Li Z, Zhao J, Liu B, et al (2016) Controlled water vapor transmission rate promotes wound-healing via wound re-epithelialization and contraction enhancement. *Sci Rep* 2016;6:24596
44. Kean T, Thanou M (2010) Biodegradation, biodistribution and toxicity of chitosan. *Adv Drug Deliv Rev* 62(1):3–11
45. Younes I, Frachet V, Rinaudo M, Jellouli K, Nasri M (2016) Cytotoxicity of chitosans with different acetylation degrees and molecular weights on bladder carcinoma cells. *Int J Biol Macromol* 84:200–207
46. Jeong KJ, Song Y, Shin HR, Kim JE, Kim J, Sun F et al (2017) In vivo study on the biocompatibility of chitosan–hydroxyapatite film depending on degree of deacetylation. *J Biomed Mater Res A* 105(6):1637–1645
47. Chen J-P, Chen S-H, Lai G-J (2012) Preparation and characterization of biomimetic silk fibroin/chitosan composite nanofibers by electrospinning for osteoblasts culture. *Nanoscale Res Lett* 7(1):170
48. Macri L, Silverstein D, Clark RA (2007) Growth factor binding to the pericellular matrix and its importance in tissue engineering. *Adv Drug Deliv Rev* 59(13):1366–1381
49. Martino MM, Briquez PS, Ranga A, Lutolf MP, Hubbell JA (2013) Heparin-binding domain of fibrin (ogen) binds growth factors and promotes tissue repair when incorporated within a synthetic matrix. *Proc Natl Acad Sci* 110(12):4563–4568
50. Sahni A, Francis CW (2000) Vascular endothelial growth factor binds to fibrinogen and fibrin and stimulates endothelial cell proliferation. *Blood* 96(12):3772–3778
51. Thomopoulos S, Zaegel M, Das R, Harwood FL, Silva MJ, Amiel D et al (2007) PDGF-BB released in tendon repair using a novel delivery system promotes cell proliferation and collagen remodeling. *J Orthop Res* 25(10):1358–1368
52. Gamal AY, Mailhot JM (2000) The effect of local delivery of PDGF-BB on attachment of human periodontal ligament fibroblasts to periodontitis-affected root surfaces—in vitro. *J Clin Periodontol* 27(5):347–353
53. Thommen R, Humar R, Misevic G, Pepper MS, Hahn AW, John M et al (1997) PDGF-BB increases endothelial migration and cord movements during angiogenesis in vitro. *J Cell Biochem* 64(3):403–413
54. Gailit J, Clarke C, Newman D, Tonnesen MG, Mosesson MW, Clark RA (1997) Human fibroblasts bind directly to fibrinogen at RGD sites through integrin $\alpha v \beta 3$. *Exp Cell Res* 232(1):118–126
55. Brown LF, Lanir N, McDonagh J, Tognazzi K, Dvorak AM, Dvorak HF (1993) Fibroblast migration in fibrin gel matrices. *Am J Pathol* 142(1):273

Submit your manuscript to a SpringerOpen[®] journal and benefit from:

- Convenient online submission
- Rigorous peer review
- Open access: articles freely available online
- High visibility within the field
- Retaining the copyright to your article

Submit your next manuscript at ► springeropen.com
